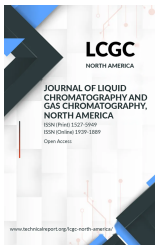

Journal of Liquid Chromatography and Gas Chromatography, North America
https://technicalreport.org/lcgc-north-america/

LC GC N. Am., Vol. 44, No.2, 12-19, 2026

Technical Reports Press

RESEARCH ARTICLE

Single Exosome Surface Enhanced Raman Spectroscopy from HEK293T Cells Using Flexible Silver Metasurfaces

Theodore L. Brown[1*] **and Mark A. Ratner**[2]

[1]*Beckman Institute for Advanced Science and Technology, Urbana, IL, USA.*
[2]*Department of Chemistry, Northwestern University, Evanston, IL, USA*
[*]*Corresponding author*

Corresponding author:
ratner@northwestern.edu

Received: 02 December 2025
Accepted: 27 April 2026
Available online: 30 June 2026

Abstract
SERS of single exosomes on flexible plasmonic substrates is the most credible when its spectroscopic interpretation is based on the physical object behind it. This study considers object gated HEK293T single exosome SERS interval ledger on flexible silver metasurface and poses the following specific question: Given the criteria of topographical and electrical eligibility, how much of the assigned Raman readout is specific evidence, and how much is mixed support? Measurement criteria include a silver metasurface with a period of 400(10) nm, modulation amplitude of 70 nm to 90 nm, vesicle compatible object scale of 30 nm to 150 nm, excitation at 785 nm and approximately 1.5 mW power, and nine assigned Raman intervals within 600 cm^{-1} to 1700 cm^{-1}. The analysis of the interval ledger includes the criteria of object eligibility, interval separation, evidence weight and ambiguity burden for the assigned neighbourhoods. Nine assigned windows cover 355 cm^{-1} out of 1100 cm^{-1} interval span, with 745 cm^{-1} remaining unassigned biochemically. The strongest protein pivots in the measurement are the windows at 810 cm^{-1} to 830 cm^{-1} and 940 cm^{-1} to 965 cm^{-1}, which have higher evidence score than the corresponding mixed windows. The high wavenumber domain 1495 cm^{-1} to 1630 cm^{-1} is the tightest local cluster (85.2 % packing density), but is not the one with the highest evidence score. The intermediate 1200 cm^{-1} to 1370 cm^{-1} region has the biologically significant content of proteins and nucleic acids, contributing to the largest ambiguity burden. Conclusion: the spectrum that passed through the gate should be interpreted as a role distributed SERS profile, where two lower-wavenumber protein pivots serve as specific evidence, the upper region provides tight biochemical context and middle region serves as mixed support.

Keywords: single exosome, extracellular vesicle, surface-enhanced Raman scattering, AFM–SSRM screening, interval evidence, ambiguity burden, flexible metasurface, HEK293T

1. Introduction

Extracellular vesicles (EVs) are membrane-bound nano-sized particles secreted by cells into the extracellular milieu [1]. The cargo of the EV includes proteins, lipids, nucleic acids, metabolites and membrane bound molecular markers, so the vesicle holds the information about the cell that generated it [2]. That is the reason why the study of exosomes and small EVs became the topic in the fields of biomarkers, intercellular communication, immune regulation, oncology and nanomedicine [3]. At the same time, the study of EVs is complex due to the presence of lipoproteins, protein aggregates, extracellular nanoparticles and preparation-related contamination along with the particles in the exosome range [4]. In large-scale EV reporting guidelines, no claim is allowed based on a single physical measure or a single molecular marker [5]. The reporting of the EV context, preparation, measurement and molecular evidence is recommended instead [6]. The caution required for EV single-particle analysis is even higher, because the results are assigned to one single nanoscale object rather than to an average vesicle preparation.

The modern studies of EV biology confirm that the exosome-like particles cannot be considered as a homogeneous set of vesicles. The proteomics and nucleic-acid studies revealed heterogeneity of the cargo

Cite as: T. L. Brown, M. A. Ratner. Single Exosome Surface Enhanced Raman Spectroscopy from HEK293T Cells Using Flexible Silver Metasurfaces. LC GC N. Am., 44(2) 2026: 12-19.

and the surface composition in small EV fractions [7]. Besides, there is a heterogeneity in the association of the particles with the extracellular material [8]. The heterogeneity in this case is not a minor technical issue for Raman or SERS analysis, since the spectrum of the one gate-passed vesicle-like object may have the detailed chemical information and yet not to be representative of the whole population. This is the reason why single-vesicle SERS analysis requires a different kind of arguments compared to a population classifier. The main goal is not to draw conclusions about the biological phenotype of a vesicle from one spectrum; the key point is to understand the exact regions assigned as specific enough for biochemical interpretation and to keep the caution in those spectral regions that overlap with others.

Raman spectroscopy is ideal for solving this problem, since it gives the vibrational information about molecular bonds without fluorescent markers and antibodies. The biological Raman bands arise from the side chains of the amino acids, vibrations of peptide backbones, nucleic acid bases, lipid chains, carotenoids or polyenes and small metabolites [9]. The reviews of the Raman spectroscopy in biology highlight the biochemical richness of this technique [10]. However, the complexity of the interpretation of crowded spectra due to the presence of proteins, lipids and nucleic acids was emphasized [11]. This remains true in the modern biological Raman analysis [12]. In turn, the problem is exacerbated for a nanoscale vesicle, since the amount of Raman active substances is low and the optical sampling volume may include the molecules adsorbed on the substrate. The direct Raman scattering is usually too weak for the single-vesicle chemical analysis, which makes the application of SERS reasonable.

SERS provides a way to enhance the Raman signal by concentrating optical field around plasmonic metal nanostructures. The foundation of the SERS is in the observations performed on roughened silver electrodes [13]. Then, the nature and the scale of the enhancement were determined [14]. Later, the single-molecule sensitivity became an important step in the SERS development [15]. SERS became a key approach in molecular sensing and plasmonic substrates [16, 17], with the emerging applications in biomedical labels and label-free bioanalysis [18]. The same enhancement mechanism poses a problem for the single-exosome interpretation, since the strong SERS signal does not imply that it comes from a vesicle. Instead, it may originate from adsorbed residues, conductive metal asperities, substrate defects or the hotspot that is not related to the biological particle at all. In this study, the eligibility of the object is considered as the first condition for chemical interpretation. Practically speaking, a nanoscale feature has to pass a topographic criterion, compatible with vesicle dimensions, and a conductive screening criterion, incompatible with the metal defect.

The studies of EVs' Raman and SERS analysis went from comparing the ensemble spectra to single-vesicle measurement and classification with the machine learning. Raman spectroscopy was applied to assess EVs' preparation purity and functionality [19], and to classify the extracellular vesicles from their Raman spectra [20]. Several studies were dedicated to the investigation of SERS signatures of single-vesicles [21]. Other particle- and plasmonic-related analyses followed this direction [22], including some single-vesicle implementations [23]. Cancer-related EVs SERS fingerprints were studied in the early diagnostic researches [24]. Later, the clinically motivated studies continued and expanded these approaches [25], including alternative platforms and sample settings [26]. The recent studies continued the above trend [27]. All these papers show that the EV spectra contain valuable biochemical information, but also reveal the dependence of the spectral interpretation on the substrate design, isolation method, preparation purity, optical setup, preprocessing and assignment strategy. In this connection, recent reviews of EVs' Raman and SERS analysis put a lot of emphasis on reproducible substrates [28], signal processing transparency [29], and careful band assignment [30]. The deterministic interval reading fits this caution, since every biochemical statement is connected to the declared interval boundaries and families. The flexible SERS substrates are especially relevant in this respect, since they can combine the plasmonic activity on the bendable or deformable substrate while maintaining the nanoscale field enhancement. The reviews of flexible SERS platforms mention paper- or polymer-based substrates [31], as well as inorganic materials [32]. The issues of uniformity and quantitative reliability are emphasized in them [33], along with the local morphology and enhancement reproducibility [34]. In the case of HEK293T single-exosome metasurface, the flexible silver relief is not just a passive substrate. The period, modulation amplitude and local depressions define the physical environment of the vesicle-scale objects positioning. The environment is important in the sense that the same plasmonic surface that enhances the signal can cause the artifacts due to misinterpretation of the conductive defects and metallic asperities as biological particles. In this respect, the combination of atomic force microscopy (AFM) and scanning spreading resistance microscopy (SSRM) serves as the gate for the spectral reading: the morphology and electric exclusion have to come before chemistry.

The basis for the HEK293T single-exosome SERS measurement performed on the flexible silver metasurface by Mochalov et al. is the physical and spectral quantities used in this study [35]. The mentioned quantities are the silver metasurface period, modulation amplitude, vesicle-compatible object scale, excitation conditions and nine assigned Raman intervals in the 600 cm^{-1} to 1700 cm^{-1} readout range. These quantities provide a role-specific biochemical interpretation of the assigned interval list. The research question posed here is specifically narrow: after the physical object eligibility is fixed, is the assigned interval list able to distinguish the regions with high specificity of protein pivots, a compact upper cluster and a broad mixed central support?

The above question is not the same as the exosome-classification question. It does not ask whether the spectrum allows classifying the disease states, predicting cell state or reconstructing the vesicle composition. Instead, it asks how the gate-passed interval list should be interpreted in order to avoid overstatement of the meaning of the broad mixed intervals. The simple peak list is not enough for this purpose, since it hides the unassigned part of the readout range. Also, the total assigned width is not enough, since the broad mixed intervals may seem more informative than the narrow selective ones. The interval interpretation adopted here avoids these issues, since it keeps the following information about the interval evident: the selectivity, width and neighbouring separation. The ambiguity burden measures how much of the assigned width is chemically nonexclusive. As a result, the interval interpretation is transparent enough to be checked from the interval boundaries directly.

Hence, the spectrum is analyzed as the role-distributed readout instead of a simple protein-enriched fingerprint. The protein pivots in the lower wavenumbers, the compact upper cluster and the broad mixed central support are considered as distinct regions due to the difference in the interval width, neighbouring separation, family selectivity and ambiguity burden.

2. Materials and Methods

2.1. Measurement Basis and Fixed Quantities

The calculations are applied to an object-gated single-exosome SERS interval ledger. The physical context is that of a flexible silver-coated metasurface used for the detection of HEK293T derived exosomes or vesicles like exosomes under excitation by light with wavelength 785 nm and power 1.5 mW. The Raman readout domain is 600 cm^{-1} to 1700 cm^{-1}. The period of the metasurface is considered to be 400(10) nm, the modulation amplitude 70 nm to 90 nm and the compatible with vesicle objects diameter range 30 nm to 150 nm.

The parameters given in Table 1 relate the nanoobject, the plasmonic surface and the spectral domain. The parameter of object-to-period relates to the fact that the vesicle-sized nanoobject occupies only a fraction of one period of the metasurface, and this is indeed a property that fits well with the locally measured depression-scale rather than an average-surface scale. The modulation parameter tells us that the relief is sufficient to affect the contact geometry and the hot spot positioning.

Table 1: Measurement quantities.

Quantity	Value	Interpretive role
Metasurface period, L	400(10) nm	Sets the lateral scale of the flexible silver relief.
Modulation amplitude, h	70 nm to 90 nm	Defines the vertical relief relevant to local object contact.
Relative modulation, h/L	0.175–0.225	Indicates that the relief depth is substantial on the vesicle scale.
Object diameter interval, d	30 nm to 150 nm	Defines the topographic size range considered vesicle compatible.
Object-to-period ratio, d/L	0.075–0.375	Relates a vesicle-scale object to one metasurface period.
Raman readout span	600 cm^{-1} to 1700 cm^{-1}	Sets the domain for interval occupancy and separation calculations.
Excitation wavelength	785 nm	Specifies the optical condition of the SERS readout.
Optical power	approximately 1.5 mW	Defines the low-power label-free measurement condition.

The ratio between modulation amplitude and metasurface period is expressed as

$$\frac{h}{L} = \frac{70\,\text{nm to } 90\,\text{nm}}{400\,\text{nm}} = 0.175\text{–}0.225. \tag{1}$$

The vesicle-to-period relation is expressed as

$$\frac{d}{L} = \frac{30\,\text{nm to } 150\,\text{nm}}{400\,\text{nm}} = 0.075\text{–}0.375. \tag{2}$$

These two dimensionless quantities are not concentration measurements. They are part of the geometric condition check. The object under consideration is small compared to the period of the metasurface, yet big enough to be regarded as a local nanoscale feature. This is why the geometric condition is the physical basis for the evaluation of object morphology and conductance prior to discussing Raman chemistry.

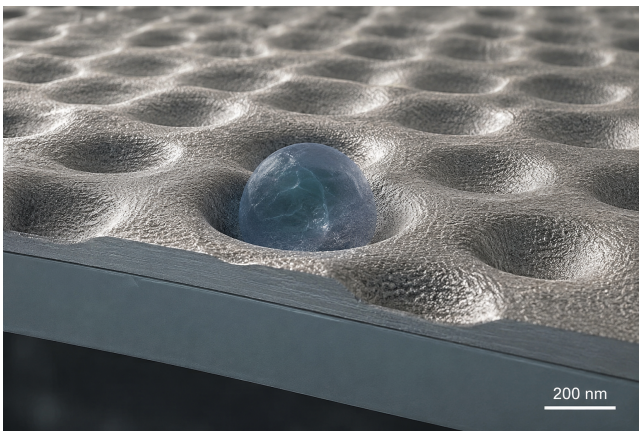

Figure 1: Metasurface contact setting.

The surface snapshot in Figure 1 provides the physical context of the data presented in Table 1. A vesicle-like particle lies within a relief environment rather than on a flat inert support. Thus, the image confirms why metasurface is considered an enhancer as well as a selection environment. Also, it serves as an illustration of why two different statements should be distinguished: the particle may be a physically eligible candidate for single-vesicle SERS but its spectrum should be interpreted at the interval level in terms of its biochemical significance.

2.2. Object Eligibility Gate

Only those candidate Raman spectra which pass the object eligibility gate are interpreted. The topographic condition, T_i, is fulfilled if the object under study is compatible with a vesicle-like nanoscale object. The conductive-screening condition, Q_i, is fulfilled if the same object does not have conductive-metal defect properties. The object gate is defined as follows:

$$\mathcal{G}_i = \mathbf{1}(T_i = 1)\mathbf{1}(Q_i = 1). \tag{3}$$

The binary product in Eq. (3) reflects the order of inference. An object that does not satisfy the conditions of vesicle-compatible topography or defect-like conductance cannot be saved by the strength of the Raman signal. On the other hand, an object that passes the gate is not automatically transformed into a compositional map. Passing the gate means that one is allowed to proceed to the next step, namely, the interval interpretation.

The height field image in Figure 2 represents the morphology part of the gate. The central object demonstrates nanoscale height signature that is compatible with the vesicle diameter interval. This is not a proof of molecular identity by itself but a condition that makes impossible to isolate the subsequent spectral reading from the physical object. In single-exosome SERS, the connection between the two is crucial because the hot spot and the object are inseparable components of the process.

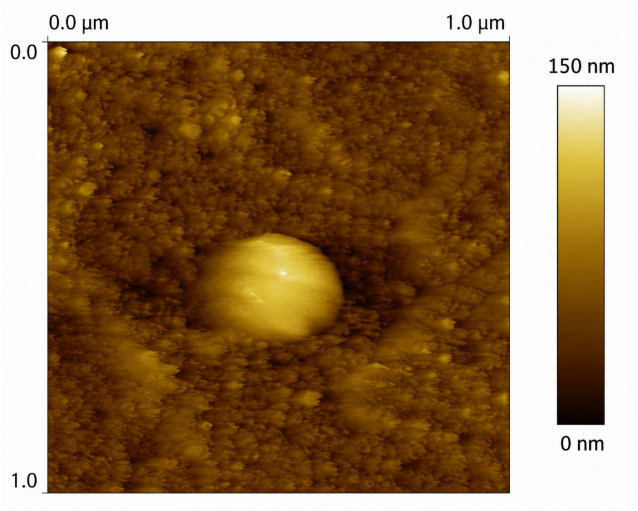

Figure 2: AFM topographic gate.

Conductance map shown in Figure 3 provides the other half of the gate. High-conducting areas could not be used for chemical identification of vesicles alone since they may represent either metallic or substrate artifacts. Thus, the low-conducting artifact-free region is critical in that case not as the chemical spectrum but rather as a negative control of any conductive artifact. This way both the topography and the SSRM images support the prudent approach: physics first, then chemistry.

2.3. Interval Ledger and Family Coding

The Raman ledger contains nine assigned windows inside the 600 cm^{-1} to 1700 cm^{-1} domain. Each interval $B_j = [\nu_j^-, \nu_j^+]$ is represented by its lower boundary, upper boundary, centre and width:

$$\bar{\nu}_j = \frac{\nu_j^- + \nu_j^+}{2}, \qquad \Delta_j = \nu_j^+ - \nu_j^-. \tag{4}$$

The Eq. (4) ensures the ledger of the interval in a way that can be validated independent of subjective peak drawing. The centre specifies

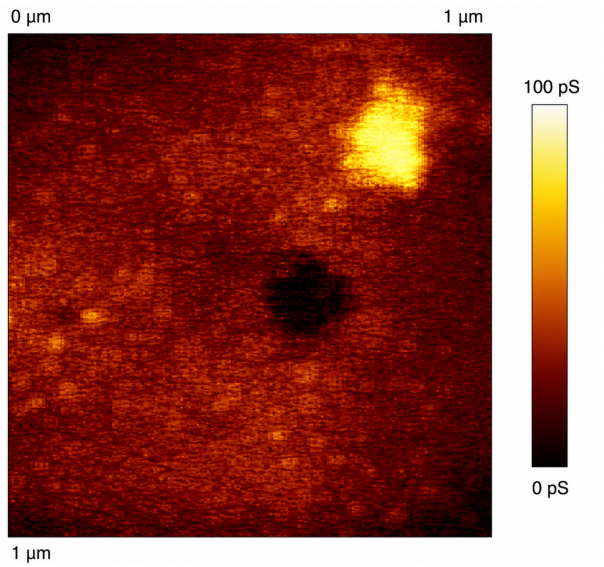

Figure 3: SSRM conductance screen.

the placement of the interval on the Raman axis while the width defines the amount of wavenumber range taken up by the interval. Wide intervals are not necessarily more indicative than narrow ones since the wide intervals may represent a wider biochemical range.

Family classification is defined by $C_j \subseteq \{P,N,L,A,M\}$ where P stands for protein, N stands for nucleic acid, L stands for lipid, A stands for carotenoid/polyene and M stands for coenzyme/metabolite vibration. Family classification is purposely nonexclusive due to the overlapping nature of biological Raman bands. The mixed interval gets listed in the ledger while ambiguity burden of being a mixture is computed later.

Chemical selectivity is defined as

$$S_j = \frac{1}{|C_j|}. \tag{5}$$

A single-family interval has $S_j = 1$, a two-family interval has $S_j = 0.5$, and a three-family interval has $S_j = 0.333$. This term is deliberately simple because it records a direct feature of the assignment: the more families attached to one interval, the less specific that interval is as a single-family molecular claim.

Width precision is defined as

$$P_j = \frac{\Delta_{\max} - \Delta_j + \Delta_{\min}}{\Delta_{\max}}, \tag{6}$$

where $\Delta_{\min} = 20$ and $\Delta_{\max} = 70$ cm^{-1} for the nine-interval ledger. Family richness is

$$R_j = \frac{\log(1+|C_j|)}{\log(4)}. \tag{7}$$

The interval-persistence score is then

$$\Pi_j = 100\left(\frac{3S_j + 2P_j + R_j}{6}\right). \tag{8}$$

Eqs. (6)–(8) separate three aspects of an assigned band: how narrow it is, how exclusive its family assignment is and whether mixed biochemical content is still present. The score is not a substitute for intensity, concentration or diagnostic probability. It is a transparent support value for a small interval ledger.

2.4. Interval Separation and Local Packing

The first structural operation describes how assigned intervals are positioned within the full readout domain. After sorting by increasing wavenumber, the left and right separations surrounding interval j are

$$s_j^- = \begin{cases} \nu_j^- - 600, & j = 1, \\ \nu_j^- - \nu_{j-1}^+, & j > 1, \end{cases} \quad s_j^+ = \begin{cases} \nu_{j+1}^- - \nu_j^+, & j < n, \\ 1700 - \nu_j^+, & j = n. \end{cases} \tag{9}$$

The local separation support term is

$$Z_j = \frac{\sqrt{(s_j^- + 1)(s_j^+ + 1)}}{\sqrt{(s_j^- + 1)(s_j^+ + 1)} + \Delta_j}. \tag{10}$$

The new unit ensures that the measure does not degenerate for small intervals. High Z_j indicates that an interval is well separated from surrounding assignments compared to the interval size. Low Z_j indicates either that the interval is enclosed in a dense cluster of assignments or that the interval is wider than its surroundings. This parameter characterizes the interval context but is not an intensity measure.

Regional packing density is defined as follows:

$$K_r = \frac{\sum_{j \in r} \Delta_j}{\max_{j \in r}(\nu_j^+) - \min_{j \in r}(\nu_j^-)}. \tag{11}$$

Spectral regions were selected based on the natural partitioning of the assignments into three groups: 715 cm^{-1} to 965 cm^{-1}, 1025 cm^{-1} to 1370 cm^{-1} and 1495 cm^{-1} to 1630 cm^{-1}. Packing density reflects the amount to which the allocated windows use the local envelope space. Packing density is not related to the total allocated width since there may be a large distance between two allocated windows.

2.5. Neighbourhood-Weighted Interval Evidence

Interval sharpness is defined as

$$H_j = \frac{\Delta_{\min}}{\Delta_j}. \tag{12}$$

The neighbourhood-weighted evidence score combines selectivity, sharpness and separation support:

$$\Psi_j = 100(0.35S_j + 0.35H_j + 0.30Z_j). \tag{13}$$

Weights retain the intrinsic interval features and the spectral local environment in one computation. Selectivity and sharpness both are assigned values of 0.35 as the interval must be chemical specific and narrow. Local discrimination is assigned 0.30 as the adjacent context is relevant, but it must not overshadow the interval's own value and width. Interpretation is ordinal in nature. An interval with high Ψ_j is a powerful evidence point. Interval with low Ψ_j also holds relevance but it must be defined in a broad manner.

2.6. Ambiguity Burden

The ambiguity burden measures how much assigned width is chemically nonexclusive:

$$A_j = \Delta_j(1 - S_j). \tag{14}$$

Intervals containing a single family contain no ambiguity burden. A two-family interval adds an ambiguity burden of one-half of its width, and a three-family interval adds an ambiguity burden of two-thirds of its width. This ensures that mixed intervals, even broad ones, are not considered as full independent evidences in each listed biochemical family.

The evidence and ambiguity measures per biochemical family are recalculated as

$$F_m = \sum_{j:m\in C_j} \frac{\Psi_j}{|C_j|}, \qquad U_m = \sum_{j:m\in C_j} \frac{A_j}{|C_j|}. \tag{15}$$

The recalculation of Eqs. (15) is not a molecular deconvolution procedure. It is simply an adjustment to account for double counting. A family can have high evidence because of the presence of narrow intervals, and it can have high ambiguity because of the presence of broad mixed intervals. Making this distinction is key to the proper interpretation.

2.7. Inference Boundaries

All the numeric measures in the tables are calculated based on the given geometry, the acquisition conditions, the interval endpoints and the chemical-family codes. No interval is interpreted in a context other than the object-gating context. Mixed intervals are characterized by their ambiguity burden and not split into single-family intervals. Therefore, the inference applies to a set of gate-passed HEK293T single-exosome intervals. The inference does not imply any vesicle concentration, clinical class, population or universal EV subtype identification. The language used below is deliberately restrictive: the two highest-evidence lower intervals are protein pivots, the upper interval is a compact cluster, and the middle one is mixed molecular support.

3. Results and Discussion

3.1. Object-Gated Measurement Context

The defined physical characteristics first confirm that the Raman interpretation is associated with a nanoscale contact phenomenon and not with free bulk spectroscopy. The period of the metasurface of $400(10)$ nm is significantly greater than the lower part of the vesicle-compatible size range, whereas the 70 nm to 90 nm modulation is sufficient to create nanoscale depressions and geometry of the local field. As a consequence, the resulting d/L ratio range of 0.075–0.375 implies that a vesicle-like object can cover a limited area of one periodic relief feature. The scale relation thus makes object gating scientifically justified: a strong Raman signal from this surface cannot be interpreted as evidence of biology unless the object has a morphology and an electrical structure compatible with it.

The first table and the first three figures interact synergically. Table 1 provides the specific numeric context; the metasurface contact figure explains why it is important on the spatial scale; the AFM and SSRM figures explain why the analysis distinguishes physical eligibility from chemical assignment. This order is crucial for the logic order since it precludes starting the Results and Discussion section with the band assignment alone. The SERS signal can be analyzed only when the object has a physical foundation.

3.2. Occupancy of Intervals and Spectral Coverage

The nine assigned Raman windows cover 355 cm^{-1} of the 1100 cm^{-1} domain of the readout from 600 cm^{-1} to 1700 cm^{-1}. The unassigned portion is 745 cm^{-1}, which equals 67.7% of the readout range. This number is not just a statistical value. It indicates that the spectrum of a single exosome is discontinuous as a biochemical record. Interpretation therefore must be based on the properties of particular assigned windows, not on the assumption that the whole spectral range contains biochemical information.

Table 2 demonstrates the reason why interpreting the width of the intervals would lead to a mistake. Two broad middle intervals, 1200 cm^{-1} to 1265 cm^{-1} and 1300 cm^{-1} to 1370 cm^{-1}, have the largest individual widths but the lowest evidence scores as they are wide and chemically mixed. Two narrow lower protein intervals, 810 cm^{-1} to 830 cm^{-1} and 940 cm^{-1} to 965 cm^{-1}, are chemically selective and separated from neighbours; hence, they have the strongest evidence. This contrast solves the main problem: the broad assigned width is not identical to the decisive molecular evidence.

Table 2: Interval ledger.

Interval	Width	Families	Π_j	Z_j	Ψ_j	A_j	Dominant assignment
715–740	25	*P,N,M*	64.3	0.784	63.2	16.7	Tryptophan, coenzyme-related band, nucleic acid.
810–830	20	*P*	91.7	0.816	94.5	0.0	Tyrosine-associated protein band.
940–965	25	*P*	89.3	0.767	86.0	0.0	Alpha-helical protein backbone contribution.
1025–1060	35	*P,L*	64.4	0.726	59.3	17.5	Protein–lipid C–N/C–C stretching.
1200–1265	65	*P,N*	50.1	0.523	44.0	32.5	Amide III and uracil-associated vibration.
1300–1370	70	*P,N*	47.7	0.490	42.2	35.0	Nucleic-acid methylene and protein-backbone deformation.
1495–1530	35	*A*	84.5	0.562	71.9	0.0	Carotenoid/polyene vibration.
1545–1570	25	*P,N*	69.2	0.282	53.9	12.5	Guanine, amide II, and tryptophan contribution.
1575–1630	55	*P*	75.0	0.273	55.9	0.0	Aromatic amino-acid vibration.

Figure 4 illustrates the discontinuity clearly. The windows of interest are not evenly spread across the 600–1700 cm^{-1} domain. Unassigned zones exist between the assigned windows, which means that the spectrum must be read as a collection of chemically relevant windows rather than as a single compositional field. This issue is especially important for SERS performed on a single object as the local enhancement favours molecules near the metallic relief while leaving all other substances unobserved.

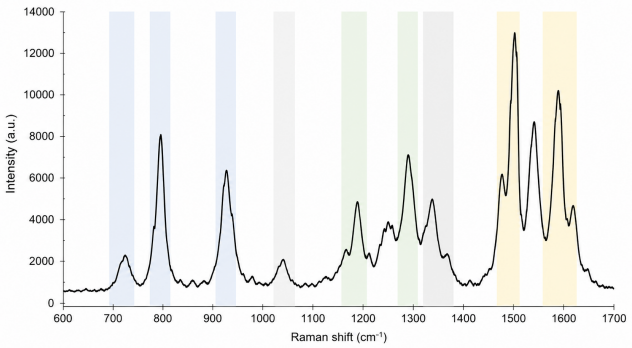

Figure 4: Gate-passed SERS readout.

Figure 5 reduces the interval table to an ordinal reading. Two highest points are located in the lower protein-associated area, while the broader central intervals are positioned lower although they have a higher width. The upper region is neither weak nor dominating: it is positioned in-between as it has both selective and crowded intervals. Therefore, the visual representation gives support to a more accurate statement than the protein dominance: the protein-associated evidence is strongest where the interval is narrow and chemically selective.

Comparison of Π_j and Ψ_j adds another dimension. Persistence score considers the width and selectivity, while the neighbourhood score takes into account the separation. That is the reason why the 1575 cm^{-1} to 1630 cm^{-1} interval is chemically significant but is not a leading point in the evidence constellation. It is single-family assigned but is included into a compact upper cluster with the short distances within the group. Thus, the conclusions obtained in Table 2 and Figure 5 are structural, not numerical. The evidence score defines which intervals should have the strongest written claims and which intervals should be considered as a context.

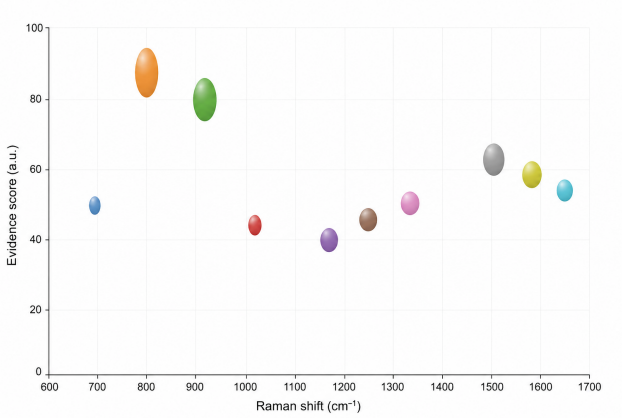

Figure 5: Evidence score map.

3.3. Regional Structure and Local Packing

In the separation structure, the readout assigned is divided into three regions. The largest separation is at 140 cm^{-1} in the range of 1060 cm^{-1} to 1200 cm^{-1}. The second-largest separation is at 125 cm^{-1} in the range of 1370 cm^{-1} to 1495 cm^{-1}. Another large separation from the lower limit to the first assigned range is 115 cm^{-1}. These large separations help distinguish the lower region with the proteins and pivot region from the middle mixed support region and separate the middle region from the upper compact cluster region. The smallest separations are 15 cm^{-1} and 5 cm^{-1}, and these are seen in the upper region, which helps to make that region locally dense although it has not the highest evidence score.

First, the regional analysis in Table 3 distinguishes between three different qualities that are frequently confused: assigned width, local density, and evidence strength. In particular, the lower region has the minimum assigned width and the lowest local packing density, but the highest mean evidence score. The middle region has the maximum assigned width but the lowest mean evidence, since its assignments are broad and mixed. The upper region has the maximum packing density since its assigned intervals fill most of a small envelope, but its mean evidence is lower than that of the lower region since its intervals are locally crowded. Such a comparison is key for the Results and Discussion since local density, total width, and interpretive strength are distinct quantities.

Table 3: Regional roles.

Region	Envelope	Assigned width	Packing density	Mean Ψ_j	Primary role
Lower, 715–965	250 cm^{-1}	70 cm^{-1}	28.0%	81.2	Protein-pivot zone
Middle, 1025–1370	345 cm^{-1}	170 cm^{-1}	49.3%	48.5	Mixed-support zone
Upper, 1495–1630	135 cm^{-1}	115 cm^{-1}	85.2%	60.6	Compact cluster

The regional representation in Figure 6 transforms the data in Table 3 into a spectral plot. The lower region is sparse but highly evidenced, the middle region is broad but chemically mixed, and the upper region is dense but locally crowded. Such an association prevents a common mistake: the densest region is not necessarily the most evident one. For a gate-passed HEK293T single-exosome spectrum, the most interpretable description would be that the lower protein pivots provide specificity, the upper cluster provides a dense biochemical context and the middle region provides broad molecular support.

At this point, special attention should be given to the middle domain. The two regions at 1200 cm^{-1} to 1265 cm^{-1} and 1300 cm^{-1} to 1370 cm^{-1} are biologically relevant because they include contributions of amides, backbone, uracil, and nucleic acids. Their low evidence scores cannot be interpreted as their irrelevancy. They rather indicate the necessity to acknowledge their chemical heterogeneity. The middle domain supports the presence of vesicle-level biochemical complexity but cannot be used as a signature of one biochemical family. This conclusion is justified by the biological Raman spectroscopy literature that confirms the overlapping of amide and nucleic acid regions [36,37]. Interpretation difficulties in complex biological samples are similar [12].

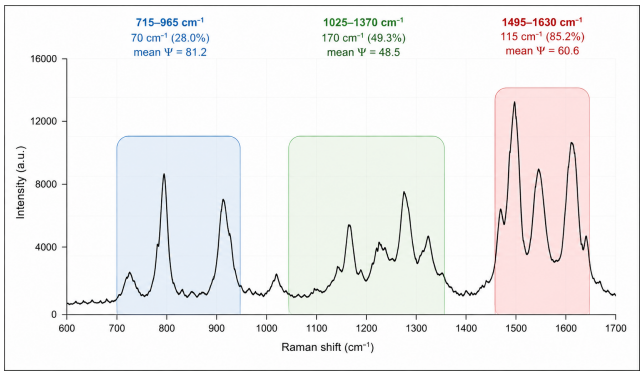

Figure 6: Regional SERS roles.

3.4. Family Evidence and Ambiguity

Family evidence redistribution reveals that the role of protein-associated chemistry is still significant, but its most powerful evidence is provided by selected intervals, rather than all protein-containing bands. The reason why the amount of evidence assigned to the protein is so high is because protein is found in two best-rated lower intervals and in some upper and mid-intervals. Nucleic-acid evidence is less important due to being obtained through mixed windows. Evidence for lipids is limited to the 1025 cm^{-1} to 1060 cm^{-1} interval; evidence for carotenoids/polyenes is limited to 1495 cm^{-1}; to 1530 cm^{-1}; coenzyme/metabolites are limited to the lower mixed interval.

The family Table 4 gives further precision to the protein conclusion. Protein has the biggest evidence share but also has a big ambiguity share since it is present in mixed windows. Nucleic acid is present in a small evidence share but has the biggest ambiguity share because its contribution comes mostly from broad mixed regions rather than from narrow selective windows. Carotenoid/polyene evidence is also smaller but has no ambiguity burden because the 1495 cm^{-1} to 1530 cm^{-1} interval is classified as a single-family contribution only. This is the main advantage of using ambiguity burden.

Table 4: Family-level evidence.

Family	Evidence	Ambiguity	Specificity pattern	Dominant interval
Protein	58.6%	43.7%	High evidence; mixed support	810–830, 940–965, 1575–1630
Nucleic acid	22.3%	54.8%	Moderate evidence; high overlap	715–740, 1200–1370, 1545–1570
Lipid	10.6%	1.7%	Local mixed contribution	1025–1060
Carotenoid/polyene	7.5%	0.0%	Selective upper-window signal	1495–1530
Coenzyme/metabolite	1.0%	0.0%	Minor lower mixed signal	715–740

From the interval ambiguity profile, presented in Figure 7, it can be seen that the main ambiguity burden is located in the middle protein–nucleic-acid region. Namely, the 1200 cm^{-1} to 1265 cm^{-1} interval adds up 32.5 cm^{-1} of ambiguity burden, whereas the 1300 cm^{-1} to 1370 cm^{-1} interval adds up 35.0 cm^{-1}. The two central mixed windows make a major contribution to the nonexclusive assignment. Thus, it becomes clear why the discussion about the middle region has a mixed molecular support rather than a decisive biochemical meaning. Ambiguity here is not some kind of extra thought, but a measured property of intervals.

Family evidence balance in Figure 8 strengthens the above conclusion on the biochemical-family level. Protein dominates in evidence share, but the red ambiguity burden prevents this dominance from becoming

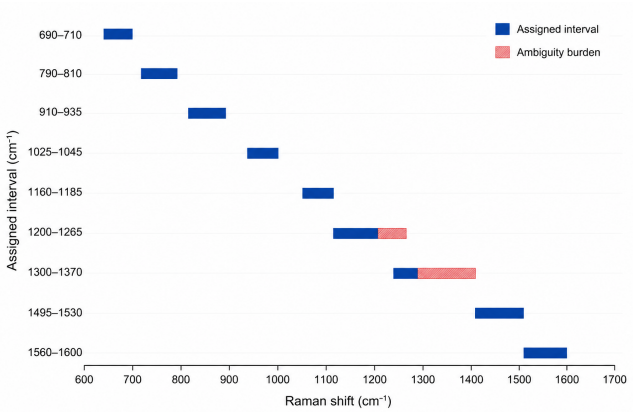

Figure 7: Ambiguity burden.

the signal of protein-only spectrum. Nucleic acid has a high ambiguity burden since it is mainly contributed by the same mixed windows with protein. Lipid, carotenoid/polyene, and coenzyme/metabolite contributions are much smaller and more local. Thus, in order to make a stronger conclusion, one needs two statements: the first is that protein chemistry is the dominant signal, and the second is that it is certain only in selected narrow windows.

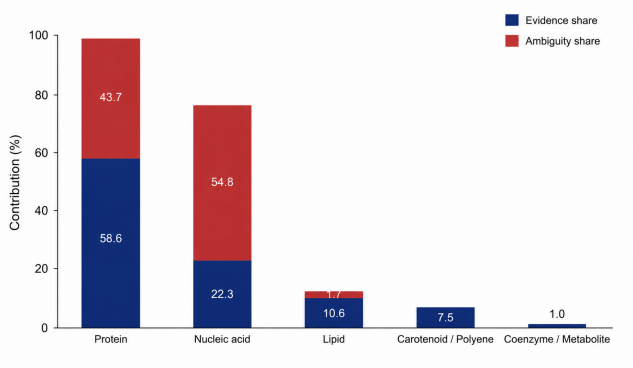

Figure 8: Family evidence balance.

3.5. Integrated Interpretation of the Gate-Passed Spectrum

All of the above results provide an answer to the research question. Object-gated interval ledger divides the intervals by their specificity. Evidence ranking defines 810 cm^{-1} to 830 cm^{-1} and 940 cm^{-1} to 965 cm^{-1} as the dominant pivots of protein. From the packing calculation, 1495 cm^{-1} to 1630 cm^{-1} emerges as the most dense local cluster with packing density of 85.2 %. From the ambiguity calculation, 1200 cm^{-1} to 1370 cm^{-1} is the one with the biggest mixed-family responsibility. The three findings above are not conflicting analyses; they are simply different aspects of the same gate-passed SERS analysis.

The last plot in Figure 9 shows the visual answer to the research question. The bottom intervals are the protein pivots with greatest specificities, the middle region is a broad but ambiguous support and the top region is a compact molecular context. The three-component reading of the data is more informative than the assertion of high spectrum protein content as it informs the reader about the location of the strongest evidence, the chemically dense region and the area with the largest nonexclusive assignment.

The interpretation also helps in planning future comparative studies of spectra of second gate-passed vesicles. A spectrum of the second gate-passed vesicle may be analyzed based on the presence of the bottom protein pivots, the unchanged compactness of the upper cluster

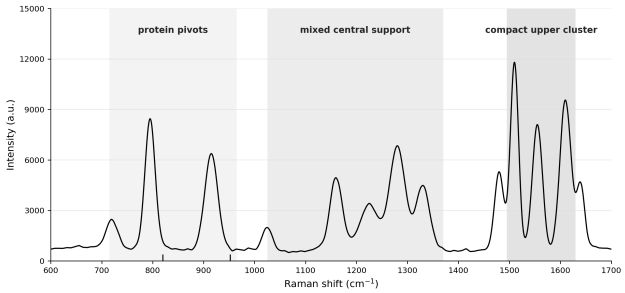

Figure 9: Region-specific interpretation.

and the change in width or ambiguity burden of the middle support band. Such approach to comparison would allow to keep the role of each interval preserved while the analysis allows careful reporting of single-object interval ledger while being ready for future replication, intensity measurement and endpoint uncertainty calculation.

The boundary of inference remains important. The analysis does not draw any conclusions on the concentration of the vesicle sample, the heterogeneity of the population, the disease state or the absolute amount of molecules. It also does not suggest that all the HEK293T-derived vesicles must have the same interval distribution. The conclusion is more specific and more definite: for the eligible physical spectrum analyzed in this paper, the assigned intervals have the specified role. The most specific chemical evidence is contained in the two lower protein intervals, the upper cluster provides the additional molecular context and the middle region provides the broad ambiguous protein-nucleic acid support.

4. Conclusions

The research question asked about the interpretation of the physically eligible HEK293T single-exosome SERS interval ledger after the AFM–SSRM object gate was satisfied. The answer to this question is that the gate-passed spectrum cannot be considered as a uniform molecular inventory. Instead, it must be analyzed as a role-distributed SERS profile where the intervals play different roles.

The first conclusion is the issue of coverage. The nine assigned windows cover the 355 cm^{-1} of the 1100 cm^{-1} readout domain leaving 745 cm^{-1} out of the biochemical ledger. This means that the spectrum is not the continuous molecular field but the set of the assigned molecular windows. The second conclusion is the issue of specificity. The intervals at 810 cm^{-1} to 830 cm^{-1} and 940 cm^{-1} to 965 cm^{-1} are the strongest protein pivots due to their narrowness, single-family assignment and favorable interval spacing. These two intervals provide the most reliable protein-specific evidence in the gate-passed readout. The third conclusion is the regional organization. The 1495 cm^{-1} to 1630 cm^{-1} region is the most compact cluster with the packing density of 85.2 % but it is not the region with the highest evidence level. The value of this region is in its biochemical compactness, not in the decision definiteness. The fourth conclusion is the issue of ambiguity. The 1200 cm^{-1} to 1370 cm^{-1} domain contains an important protein–nucleic-acid evidence but also the biggest ambiguity burden. Thus, it should be called the mixed molecular support and not the pure marker of one of the families.

In sum, these findings answer the research question. When the object eligibility is checked, the assigned intervals may be divided into high-specificity protein pivots, the compact upper biochemical cluster and the broad middle support band. The method does not transform the single-spectrum evidence into the EV population classifier and does not claim the full composition of the vesicle. Nevertheless, it allows disciplined interpretation of the evidence provided by the gate-passed single-exosome SERS ledger. The main conclusion, therefore, is not

protein domination but the reliable protein chemistry in narrow and specific intervals, the upper cluster providing the molecular context and the middle domain needing cautious interpretation due to its ambiguous biochemical meaning.

References

[1] Welsh, J. A., Goberdhan, D. C., O'Driscoll, L., Buzas, E. I., Blenkiron, C., Bussolati, B., ... & Benedikter, B. J. (2024). Minimal information for studies of extracellular vesicles (MISEV2023): From basic to advanced approaches. Journal of extracellular vesicles, 13(2), e12404.

[2] Kalluri, R., & LeBleu, V. S. (2020). The biology, function, and biomedical applications of exosomes. science, 367(6478), eaau6977.

[3] Hendrix, A., Lippens, L., Pinheiro, C., Théry, C., Martin-Jaular, L., Lötvall, J., ... & Witwer, K. W. (2023). Extracellular vesicle analysis. Nature Reviews Methods Primers, 3(1), 56.

[4] Yáñez-Mó, M., Siljander, P. R. M., Andreu, Z., Bedina Zavec, A., Borràs, F. E., Buzas, E. I., ... & De Wever, O. (2015). Biological properties of extracellular vesicles and their physiological functions. Journal of extracellular vesicles, 4(1), 27066.

[5] Mathieu, M., Martin-Jaular, L., Lavieu, G., & Théry, C. (2019). Specificities of secretion and uptake of exosomes and other extracellular vesicles for cell-to-cell communication. Nature cell biology, 21(1), 9-17.

[6] van Niel, G., Carter, D. R., Clayton, A., Lambert, D. W., Raposo, G., & Vader, P. (2022). Challenges and directions in studying cell–cell communication by extracellular vesicles. Nature reviews Molecular cell biology, 23(5), 369-382.

[7] Jeppesen, D. K., Fenix, A. M., Franklin, J. L., Higginbotham, J. N., Zhang, Q., Zimmerman, L. J., ... & Coffey, R. J. (2019). Reassessment of exosome composition. Cell, 177(2), 428-445.

[8] Kowal, J., Arras, G., Colombo, M., Jouve, M., Morath, J. P., Primdal-Bengtson, B., ... & Théry, C. (2016). Proteomic comparison defines novel markers to characterize heterogeneous populations of extracellular vesicle subtypes. Proceedings of the National Academy of Sciences, 113(8), E968-E977.

[9] Czamara, K., Majzner, K., Pacia, M. Z., Kochan, K., Kaczor, A., & Baranska, E. M. (2015). Raman spectroscopy of lipids: a review. Journal of Raman spectroscopy, 46(1), 4-20.

[10] Bocklitz, T. W., Guo, S., Ryabchykov, O., Vogler, N., & Popp, J. (2016). Raman based molecular imaging and analytics: a magic bullet for biomedical applications!?. Analytical chemistry, 88(1), 133-151.

[11] Shipp, D. W., Sinjab, F., & Notingher, I. (2017). Raman spectroscopy: techniques and applications in the life sciences. Advances in Optics and Photonics, 9(2), 315-428.

[12] Chandra, A., Kumar, V., Garnaik, U. C., Dada, R., Qamar, I., Goel, V. K., & Agarwal, S. (2024). Unveiling the molecular secrets: a comprehensive review of Raman spectroscopy in biological research. ACS omega, 9(51), 50049-50063.

[13] Fleischmann, M., Hendra, P. J., & McQuillan, A. J. (1974). Raman spectra of pyridine adsorbed at a silver electrode. Chemical physics letters, 26(2), 163-166.

[14] Albrecht, M. G., & Creighton, J. A. (1977). Anomalously intense Raman spectra of pyridine at a silver electrode. Journal of the american chemical society, 99(15), 5215-5217.

[15] Nie, S., & Emory, S. R. (1997). Probing single molecules and single nanoparticles by surface-enhanced Raman scattering. science, 275(5303), 1102-1106.

[16] Le Ru, E. C., & Etchegoin, P. G. (2012). Single-molecule surface-enhanced Raman spectroscopy. Annual review of physical chemistry, 63(1), 65-87.

[17] Schlücker, S. (2014). Surface-Enhanced raman spectroscopy: Concepts and chemical applications. Angewandte Chemie International Edition, 53(19), 4756-4795.

[18] Yi, J., You, E. M., Hu, R., Wu, D. Y., Liu, G. K., Yang, Z. L., ... & Tian, Z. Q. (2025). Surface-enhanced Raman spectroscopy: a half-century historical perspective. Chemical Society Reviews, 54(3), 1453-1551.

[19] Gualerzi, A., Kooijmans, S. A. A., Niada, S., Picciolini, S., Brini, A. T., Camussi, G., & Bedoni, M. (2019). Raman spectroscopy as a quick tool to assess purity of extracellular vesicle preparations and predict their functionality. Journal of extracellular vesicles, 8(1), 1568780.

[20] Jensen, M. N., Guerreiro, E. M., Enciso-Martinez, A., Kruglik, S. G., Otto, C., Snir, O., ... & Hellesø, O. G. (2024). Identification of extracellular vesicles from their Raman spectra via self-supervised learning. Scientific reports, 14(1), 6791.

[21] Liu, Z., Ng, M., Srivastava, S., Li, T., Liu, J., Phu, T. A., ... & Xie, Y. H. (2024). Label-free single-vesicle based surface enhanced Raman spectroscopy: A robust approach for investigating the biomolecular composition of small extracellular vesicles. Plos one, 19(6), e0305418.

[22] Parlatan, U., Ozen, M. O., Kecoglu, I., Koyuncu, B., Torun, H., Khalafkhany, D., ... & Demirci, U. (2023). Label-free identification of exosomes using raman spectroscopy and machine learning. Small, 19(9), 2205519.

[23] Kim, S., Choi, B. H., Shin, H., Kwon, K., Lee, S. Y., Yoon, H. B., ... & Choi, Y. (2023). Plasma exosome analysis for protein mutation identification using a combination of raman spectroscopy and deep learning. ACS sensors, 8(6), 2391-2400.

[24] Lee, W., Nanou, A., Rikkert, L., Coumans, F. A., Otto, C., Terstappen, L. W., & Offerhaus, H. L. (2018). Label-free prostate cancer detection by characterization of extracellular vesicles using raman spectroscopy. Analytical chemistry, 90(19), 11290-11296.

[25] Shin, H., Oh, S., Hong, S., Kang, M., Kang, D., Ji, Y. G., ... & Choi, Y. (2020). Early-stage lung cancer diagnosis by deep learning-based spectroscopic analysis of circulating exosomes. ACS nano, 14(5), 5435-5444.

[26] Banaei, N., Moshfegh, J., & Kim, B. (2021). Surface enhanced Raman spectroscopy-based immunoassay detection of tumor-derived extracellular vesicles to differentiate pancreatic cancers from chronic pancreatitis. Journal of Raman Spectroscopy, 52(11), 1810-1819.

[27] Liu, Y., Li, M., Liu, H., Kang, C., & Wang, C. (2024). Cancer diagnosis using label-free SERS-based exosome analysis. Theranostics, 14(5), 1966.

[28] Yaraki, M. T., Tukova, A., & Wang, Y. (2022). Emerging SERS biosensors for the analysis of cells and extracellular vesicles. Nanoscale, 14(41), 15242-15268.

[29] Bhowmik, D., Patel, M. T., & Goldberg Oppenheimer, P. (2025). Illuminating extracellular nanovesicles through the spectroscopic lens: a mini review of cutting-edge insights and emerging applications. Frontiers in Bioengineering and Biotechnology, 13, 1592391.

[30] Liu, Y. J., Kyne, M., Kang, C., & Wang, C. (2025). Raman spectroscopy in extracellular vesicles analysis: techniques, applications and advancements. Biosensors and Bioelectronics, 270, 116970.

[31] Laing, S., Jamieson, L. E., Faulds, K., & Graham, D. (2017). Surface-enhanced Raman spectroscopy for in vivo biosensing. Nature Reviews Chemistry, 1(8), 0060.

[32] Shvalya, V., Filipič, G., Zavašnik, J., Abdulhalim, I., & Cvelbar, U. (2020). Surface-enhanced Raman spectroscopy for chemical and biological sensing using nanoplasmonics: The relevance of interparticle spacing and surface morphology. Applied Physics Reviews, 7(3).

[33] Liu, H., He, Y., & Cao, K. (2021). Flexible surface-enhanced Raman scattering substrates: A review on constructions, applications, and challenges. Advanced Materials Interfaces, 8(21), 2100982.

[34] Liu, L., Martinez Pancorbo, P., Xiao, T. H., Noguchi, S., Marumi, M., Segawa, H., ... & Goda, K. (2022). Highly scalable, wearable surface-enhanced Raman spectroscopy. Advanced Optical Materials, 10(17), 2200054.

[35] Mochalov, K., Korzhov, D., Shestopalova, M., Ivanov, A., Afanasev, K., Smyk, A., ... & Sarychev, A. K. (2025). Single-Exosome SERS Detection by Means of a Flexible Metasurface. Biosensors, 15(12), 815.

[36] Movasaghi, Z., Rehman, S., & Rehman, I. U. (2007). Raman spectroscopy of biological tissues. Applied Spectroscopy Reviews, 42(5), 493-541.

[37] Talari, A. C. S., Movasaghi, Z., Rehman, S., & Rehman, I. U. (2015). Raman spectroscopy of biological tissues. Applied spectroscopy reviews, 50(1), 46-111.